Ion composition produced by high power impulse magnetron sputtering discharges near the substrate

A. P. Ehiasarian,[1,a)] A. Vetushka,[1] A. Hecimovic,[1] and S. Konstantinidis[2]
[1]*Materials and Engineering Research Institute, Sheffield Hallam University, Howard Street, Sheffield S1 1WB, United Kingdom*
[2]*Materia Nova, Avenue Copernic 1, 7000 Mons, Belgium*

(Received 3 June 2008; accepted 27 August 2008; published online 27 October 2008)

Plasma composition near the substrate was investigated in a high power impulse magnetron sputtering (HIPIMS) discharge using Langmuir probe analysis, mass spectroscopy, and atomic absorption spectroscopy. The HIPIMS discharge was operated in nonreactive Ar atmosphere at a pressure of 2.66 Pa and the magnetron cathode was furnished with Ti target. Plasma density, metal ion-to-neutral ratio, and gas ion-to-metal ion ratio were studied as a function of discharge current. At peak discharge current densities of ~ 1 A cm^{-2}, the results show that a dense plasma ($n_e \sim 10^{18}$ m^{-3}) expanded from the target toward the substrate and lasted more than 330 μs after the supplied power was turned off. The shape of the time-averaged ion energy distribution function of sputtered material exhibited a transition from Thompson to Maxwellian distribution, indicating efficient energy transfer in the discharge. The metal content in the plasma monotonically increased with discharge current and the metal ion-to-neutral ratio reached approximately 1:1 in the postdischarge plasma at peak current density of 5 A cm^{-2}. © *2008 American Institute of Physics*. [DOI: 10.1063/1.3000446]

I. INTRODUCTION

High power impulse magnetron sputtering (HIPIMS) is gaining acceptance in a growing number of applications such as adhesion enhancement of cutting tools used for machining Al and Ti and for dry high speed milling of hardened steel. Thin films deposited by HIPIMS exhibit dense microstructure and perform well in wear,[1] oxidation,[2] and corrosion environments.[3]

Along the coating development process, a lot of work has been done to measure and understand the plasma parameters in HIPIMS discharges. The ion and neutral densities in HIPIMS of Ti as a function of time and the transport mechanisms of ions and neutrals in the postdischarge were studied by atomic absorption spectroscopy (AAS).[4,5] The peak plasma density within the HIPIMS pulse was estimated to be $\sim 10^{19}$ m^{-3} by Langmuir probe measurements.[6] Significant metal ionization and presence of doubly charged metal ions has been detected in the HIPIMS discharge by optical emission spectroscopy (OES).[7] Ion energy distribution functions (IEDFs) of metal ions close to the target exhibited a high energy tail extending to 100 eV.[8] Near the substrate, IEDFs extended up to 60 eV with 90% of ions exhibiting energy of <10 eV.[9,10] Qualitative measurements based on OES (Ref. 11) have shown that the ion-to-neutral ratio near the target increased monotonically with peak discharge current I_d. Ti ionization degree in the vicinity of the target has been estimated by OES to be 90% (Ref. 11) at discharge current densities above 1 A cm^{-2}.

Although the temporal evolution of plasma parameters during the pulse and near the target is studied in great detail, there is limited information about the effect of discharge current on the plasma composition near the substrate. This study combines quantitative plasma diagnostic techniques such as Langmuir probe, energy-resolved mass spectroscopy, and AAS to evaluate plasma parameters in the vicinity of the substrate.

II. EXPERIMENTAL DETAILS

All experiments were carried out in a CMS-18 Vacuum System (Kurt J. Lesker Ltd.). The chamber was evacuated to a base pressure of 10^{-5} Pa by a turbomolecular pump. Figure 1 is a schematic cross section of the deposition chamber outfitted with a hollow cathode lamp and fiber optic cable used for AAS measurements. The position of the plasma-sampling mass spectrometer is also indicated; however, its

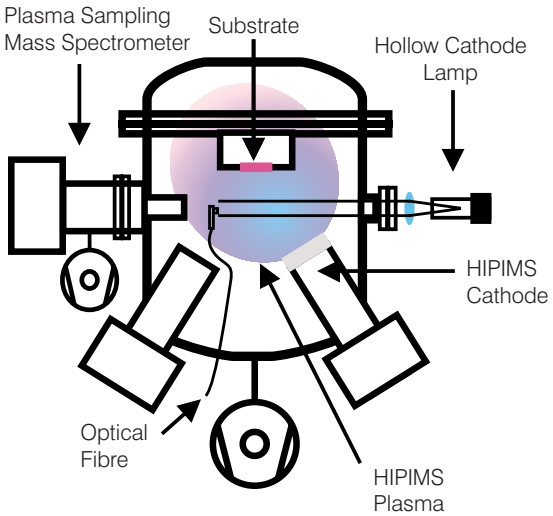

FIG. 1. (Color online) Schematic of experimental setup with AAS.

[a)]Electronic mail: a.ehiasarian@shu.ac.uk.

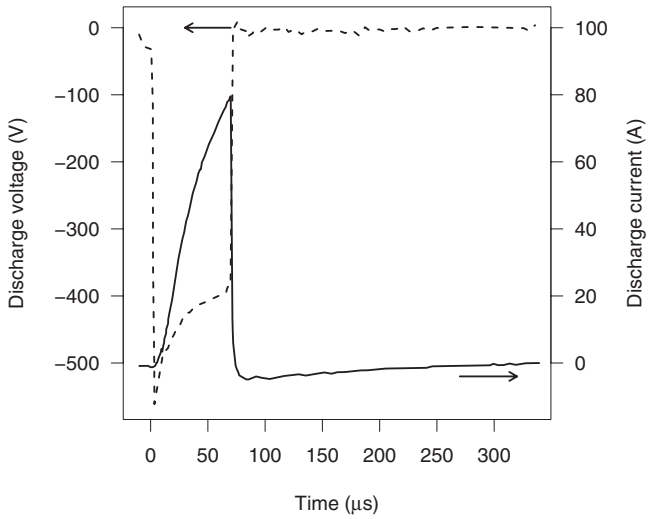

FIG. 2. Typical current and voltage waveforms of HIPIMS discharge.

real orientation was rotated to 45° with respect to the vertical axis of symmetry of the chamber. One of the magnetron sources was furnished with a titanium (Ti) target with a diameter of 75 mm and its plane was tilted at an angle of 32° with respect to the substrate plane. The discharge was driven by a dedicated HIPIMS power supply HMP 2/3 (Hüttinger Electronic Sp. z o.o.-formerly Advanced Converters) with active arc suppression. The power was supplied in unipolar rectangular voltage pulses in a frequency range of 50–100 Hz, duty cycle of 0.3%–0.7%, and pulse duration of 70 μs. The voltage was adjusted to obtain a peak discharge current density in the range of 1–5 A cm^{-2}. Typical voltage and current pulse shapes are shown in Fig. 2. We define $t=0$ as the moment when the voltage pulse was applied. The measurements were obtained in nonreactive Ar atmosphere at a pressure of 2.66 Pa.

The plasma composition near the substrate was evaluated by Langmuir probe, mass spectrometry, and AAS. All measurements were carried out in the plane of the substrate as illustrated for AAS in Fig. 1.

A. Langmuir probe measurements

A cylindrical Langmuir probe was used to obtain temporal evolution of electron density and effective electron temperature during the voltage pulse and in the postdischarge. The probe comprised a tungsten wire (150 μm diameter and 10 mm length) and was positioned at a distance of 100 mm above the magnetron in the plane of the AAS measurement indicated in Fig. 1. At this position, the magnetic field strength was ~1 mT. At the given magnetic field strength, the Larmor radius of electrons with $T_e \sim 2$ eV is $r_L \sim 3.4$ mm. Since r_L was greater than the probe radius, it was assumed that the influence of magnetic field on electron collection was negligible. The probe was connected to an automated data acquisition system ESPION (Hiden Analytical Ltd.) whose measurements were synchronized with the HMP 2/3 power supply unit. Time-resolved measurements were obtained by boxcar averaging of 60 pulses. The ESPION internal delay generator scanned through the pulse and collected a complete current-voltage (*I-V*) probe characteristics for each chosen time within the pulse. The time interval between measurements was 20 μs. To ensure the cleanliness of the probe surface, a negative voltage of −150 V was applied for a short period of time between the measurements to sputter off any deposited material.

Once the experimental data was collected, the plasma potential was determined from the zero crossing of the second derivative of the probe current with respect to voltage. The electron energy distribution function (EEDF), $F(V)$ was obtained by numerically differentiating the *I-V* curve and applying the following Druyvesteyn method:[12]

$$F(V) = \frac{1}{A_p}\sqrt{\frac{8m}{e^3}}\sqrt{V}\frac{d^2I}{dV^2}, \tag{1}$$

where A_p is the area of the probe, m is the electron mass, and e is the electron charge. The electron density n_e was calculated from the integral of the EEDF as follows:

$$n_e = \int_0^\infty F(\varepsilon)d\varepsilon. \tag{2}$$

The effective electron temperature T_e was calculated from the average energy of the EEDF as follows:

$$T_e = \frac{2}{3}\langle\varepsilon\rangle = \frac{2}{3n_e}\int_0^\infty \varepsilon F(\varepsilon)d\varepsilon. \tag{3}$$

Since the probe was placed 100 mm away from the target (i.e., in bulk plasma), it is assumed that the plasma is quasineutral there, and therefore the electron density equals the ion density at this position.

B. Mass spectroscopy measurements

Mass spectroscopy measurements were carried out to obtain IEDFs at the position of the substrate. A plasma-sampling energy-resolved mass spectrometer PSM003 (Hiden Analytical Ltd.) was mounted at a distance of 150 mm from the target. Ions were extracted through a 200 μm diameter grounded orifice oriented at an angle of 58° with respect to the normal of the target. Since the acceptance angle of the instrument was 1°, the current configuration did not allow line-of-sight detection of ions, and ions had to undergo at least one collision to be detected. This indicates that high-energy ions may not be detected. However, at the pressures discussed, the mean free path at a pressure of 2.66 Pa, was 70 mm, and therefore the majority of ions would indeed undergo at least one collision prior to reaching the mass spectrometer. The time-averaged IEDF was measured for each of the following ions: Ar^{1+}, Ar^{2+}, Ti^{1+}, and Ti^{2+}. The ratio of ion densities was determined from the ratio of the integral of each IEDF.

As the experiments were carried out at high pressure, the ions experienced a number of collisions before reaching the mass spectrometer and may be assumed to be thermalized. Thus, the obtained IEDFs were assumed and approximated to a Maxwellian distribution given by

$$F_M \approx C_1 \sqrt{\frac{\varepsilon}{(k_B T)^3}} \exp(-\varepsilon/k_B T), \tag{4}$$

where C_1 is a constant, ε is the ion energy, and $k_B T$ may be defined as the "effective ion temperature." Adopting the procedure proposed by Godyak *et al.*[13] to ions, $k_B T$ was determined from the ion energy probability function (IEPF), $f(\varepsilon)=\varepsilon^{-1/2}F_M(\varepsilon)$. Taking the logarithm and combining with Eq. (4), we obtain

$$\ln[f(\varepsilon)] = \ln(C) - 1.5\ln(k_B T) - \varepsilon/k_B T, \tag{5}$$

which is a linear relationship between the logarithm of the IEPF and ion energy ε. The slope is defined as $-1/k_B T$ and can be used to calculate the effective ion temperature. The values obtained for $k_B T$ were then inserted in Eq. (4) and the constant C_1 was determined by a least-squares fit to the experimental data. In some cases, the sum of two Maxwellian distributions was used to fit the experimental data,

$$F(\varepsilon) \approx C_1 \sqrt{\frac{\varepsilon}{(k_B T_1)^3}} \exp(-\varepsilon/k_B T_1) + C_2 \sqrt{\frac{\varepsilon}{(k_B T_2)^3}} \exp(-\varepsilon/k_B T_2). \tag{6}$$

C. Atomic absorption spectroscopy measurements

Time-resolved AAS was employed to probe the composition of the postdischarge. A Ti hollow cathode lamp was used as a light source. The lamp was driven in pulsed mode with short high-power pulses (giant pulses) providing not only Ti neutral (Ti I) but also Ti ion (Ti II) emission lines.[14] A lens was used to produce a parallel beam of light through the chamber. The light was collected with a fiber optic cable positioned at the far end of the substrate. The emission intensities were then analyzed by a Jobin–Yvon spectrometer TRIAX 320 with resolution of 0.12 nm and the signal from a selected line was recorded with an oscilloscope. Two lines were monitored: Ti I at 363.55 nm and Ti II at 338.38 nm.

In contrast to OES, the AAS method probes nonradiative species thus eliminating variations in the excitation mechanism. AAS allows the determination of absolute number densities of absorbing atoms and ions. Although basic principles and calculations involved in absorption spectroscopy can be found elsewhere,[14] one can shortly summarize its principle. Experimentally, the absorption coefficient A is obtained by measuring the intensity I_0 emitted by the lamp and the light beam intensity I_t transmitted after crossing the plasma,

$$A = 1 - \frac{I_t}{I_0}. \tag{7}$$

From this absorption coefficient, the absolute density can be determined through calculations. Once the absorption coefficients were determined for each investigated line, their ratio was used to estimate the ionization degree for Ti near the substrate.

The atom densities represent an average along the absorption length, which can be assumed being equal to the vacuum chamber diameter (500 mm). The calculation treats the case of uniform distribution along the absorption length, which is not accurate. Particularly when comparing the Ti^0 and Ti^{1+} ions, errors could be generated due to their different distribution within the chamber volume. Neutrals are affected by elastic collisions with background gas, whereas the distribution of ions is expected to follow that of the electrons and thus might be more confined within the magnetic field trap. However, the AAS measurements were taken at high gas pressure of 2.9 Pa in order to thermalize the species. In these conditions, both ions and electrons undergo numerous collisions with the gas which facilitate escape from the magnetic confinement field and probably approach the spatial distribution of sputtered neutrals.

The accurate determination of density requires that the Doppler line broadening of the absorbing line must be estimated beforehand as the line width is a parameter in the density calculation. In the present (post)discharge conditions, the line profile is related to the kinetic temperature of the absorbing species, i.e., their velocity. Since the measurements are carried out near the substrate at a high pressure of 2.66 Pa, it is reasonable to assume that Ti neutral sputtered particles are thermalized, and therefore are at a temperature close to room temperature. Indeed, the distance × pressure product is high enough and sputtered particles encounter a number of collisions with the background gas. However, titanium ions are expected to travel to the substrate faster as their speed is governed by ambipolar diffusion.[4] This temperature can be estimated from previous studies carried out in HIPIMS discharge.[4,15,16] At 6 cm from the target, at 1 Pa the metal and gas ion drift velocity was estimated by flat probes[15] to be 2500 ms^{-1}. Flat probe measurements conducted 8 cm away from the target surface[16] showed that titanium ions had a speed of ~1200 ms^{-1} at 1.3 Pa and ~220 ms^{-1} at 4 Pa. The ambipolar diffusion coefficient for Ti^{1+} is factor two higher than for Ti^0 as determined by AAS.[4] Moreover, the density evolutions published by de Poucques *et al.*[4] show that the maximum density of Ti^{1+} appears earlier Ti^0. This suggests that metal ions effectively travel faster than neutral metal atoms. From these published results, it is reasonable to assume that the metal ions at 2.66 Pa would cross the interelectrode gap at an average speed of 600 ms^{-1}, which corresponds to a kinetic temperature of 1000 K. Titanium neutrals are slower by a factor of two and diffuse at a speed of 300 ms^{-1} (kinetic temperature of 300 K). This was further confirmed by direct measurements of the IEDF for Ti^{1+} ions by energy-resolved mass spectroscopy.

III. RESULTS AND DISCUSSION

A. Plasma density

Figure 3 shows the temporal evolution of plasma density at discharge currents of 14, 40, and 80 A. The density profile exhibits two peaks–one coincides with the maximum of discharge current at $t=70$ μs and the other peak appears at $t=150$ μs. The ratio of maximum intensities of these two peaks changes as the discharge current increases. Thus at 14 A, the first peak of plasma density reaches a value of 1.1×10^{17} m^{-3} and the second peak is higher at around 1.3

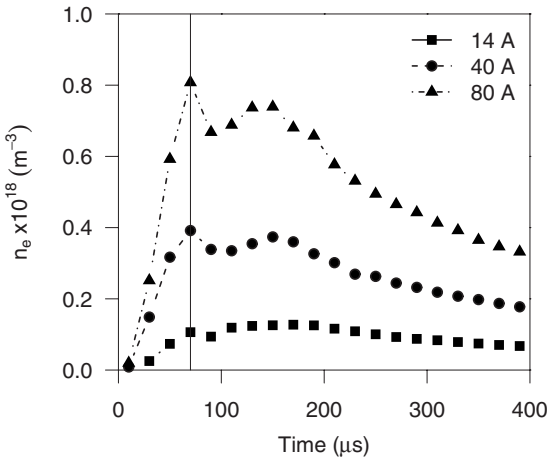

FIG. 3. Temporal evolution of electron density at I_d=14, 40, and 80 A. Vertical line indicates end of the pulse t=70 μs.

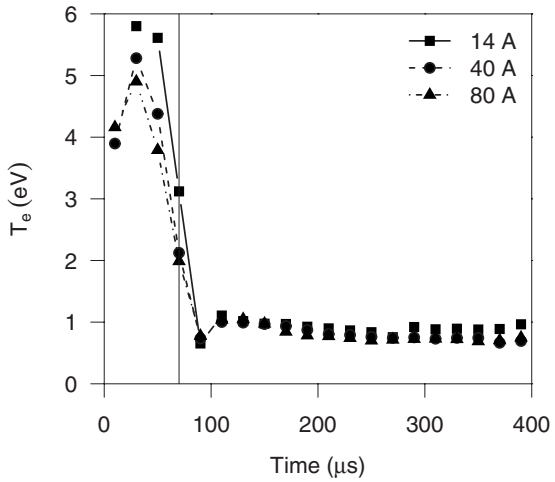

FIG. 4. Temporal evolution of effective electron temperature at I_d=14, 40, and 80 A. Vertical line indicates end of the pulse t=70 μs.

$\times 10^{17}$ m^{-3}. When the discharge current is increased to 80 A, the situation is reversed and the first peak reaches value of 8.1×10^{17} m^{-3} while the second peak is only 7.4 $\times 10^{17}$ m^{-3}. The appearance of the first peak may be attributed to the generation of argon ions via direct electron impact ionization in the vicinity of the probe. As the discharge current rises, more electrons become available to ionize argon gas, and therefore the amplitude of the first peak increases with I_d. The second peak is related to the diffusion of bulk plasma established near the target and contains both metal and gas ions. The large delay in the arrival of the second peak compared to the time of application of the pulse is attributed to the slow speed of diffusion through the gas under high pressure due to a number of elastic collisions. It should be noted that the relatively high density of the first peak compared to the second peak may be due to the high Ar pressure and an associated increased ionization probability. At the same time, with increasing I_d, stronger gas rarefaction takes place in the vicinity of the target, pushing Ar gas atoms toward the substrate, where they can be ionized. Despite diffusion, expansion and decay processes occurring between the target and substrate position, the plasma density remains at quite high level of $(0.7–3.3)\times10^{17}$ m^{-3} after 320 μs of application of the voltage pulse.

Figure 4 shows the time evolution of the effective electron temperature T_e at different discharge currents. In the beginning of the pulse, quite high values of T_e in the range 4–6 eV are observed, corresponding to the appearance of very energetic electrons ($E\sim12$ eV) in the discharge.[17] It is expected that T_e is even greater in the vicinity of the target and is gradually decreased as electrons diffuse toward the probe 100 mm away. Such hot electrons are detected throughout the pulse on time and are the main factor contributing to the ionization of metal and gas neutrals. At the end of the pulse, when the discharge current reaches its maximum value, the effective electron temperature decreases to values of ~0.7 eV as a result of a high frequency of collisions in the dense plasma and higher content of sputtered metal vapor in the chamber.

It is interesting to note that the discharge current causes variations in T_e mainly during the time when voltage is applied (i.e., in the first 70 μs). These variations are driven by hot groups of electrons that are generated by at least two mechanisms. A group of hot electrons is generated during the discharge breakdown phase.[17] Its energy strongly depends on the voltage and is expected to increase significantly as the discharge voltage increases from −400 V (−550 V in overshoot) (I_d=14 A) to −490 V (−720 V in overshoot) (I_d =80 A). A second hot group originates from energetic electrons, which have been able to escape from the vicinity of the target along unbalancing field lines. This group is representative of the plasma discharge during its ionization stage and as such is directly linked to the ionization degree in the plasma. The energy distribution of the second group is strongly modified by collisions in the plasma and is expected to decrease as a function of plasma density despite the associated increase in discharge voltage. Although the two hot groups are produced sequentially, they diffuse at different rates and are indistinguishable by the probe. Nevertheless, it may be assumed that the measured variations of T_e of 50% are an upper limit. On the other hand, the bulk plasma supports temperatures of the order of 2 eV, which remain constant as the current changes from 14 to 80 A. Moreover as shown in Fig. 3, the ion dose collected in the subsequent time between 70 and 300 μs is factor 10 greater than the dose prior, thus the majority of ions are collected in conditions of constant electron temperature of the order of 2 eV. This low energy indicates that ionization events in the expanding plasma are strongly reduced thus the plasma ionization degree is "frozen" as observed by de Poucques *et al.*[4] and Anders.[18]

B. Ion energy

The IEDFs of Ti^{1+}, Ti^{2+}, Ar^{1+}, and Ar^{2+} obtained from energy-resolved mass spectroscopy at I_d=40 A are shown in Figs. 5(a)–5(d), respectively. The dashed curves represent experimental data and the solid curves represent Maxwellian fits to it. The observed IEDF of Ti^{1+} [Fig. 5(a)] is quite narrow with 99.9% of ions having energy below 3 eV and comprises a low energy and a high energy component. The low energy part may be described with an effective ion tem-

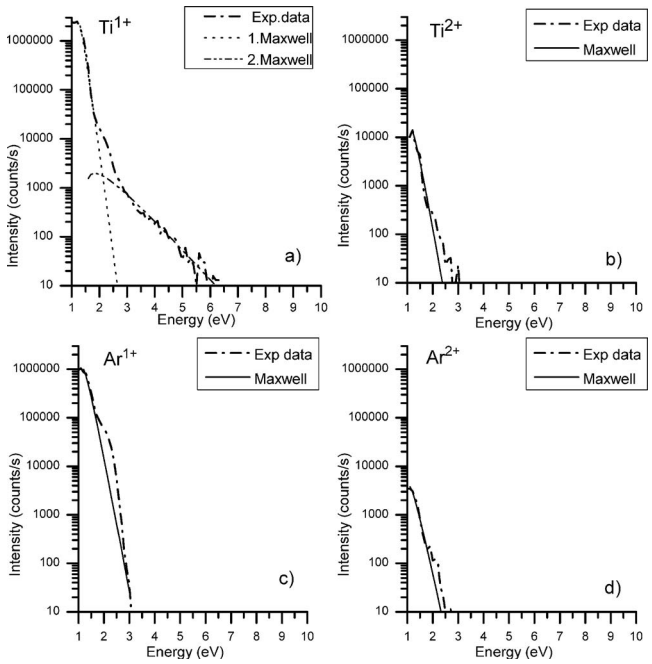

FIG. 5. Time-averaged ion energy distribution of (a) Ti^{1+}, (b) Ti^{2+}, (c) Ar^{1+}, and (d) Ar^{2+}.

perature of $k_BT=0.09$ eV and represents the majority of collected Ti^{1+} ions. This energy is sufficiently low to neglect Doppler broadening during absorption measurements. The high energy part had $k_BT=0.6$ eV. Since measurements were carried out in time-averaged mode, the resulting IEDF comprised ions collected during the pulse as well as between the pulses. The high energy tail has been attributed to ions generated during the pulse from electron ionization of Ti atoms, which carry their energy from the sputtering process.[19] This assumption was confirmed by a decrease in the fraction of high energy ions as the discharge current was decreased (not shown here). Passing through the plasma sputtered atoms are partially thermalized through collisions with the process gas thus transforming their initial Thomson energy distribution into a more randomized Maxwellian. The low energy part corresponds to ions that have been completely thermalized in collisions mainly during the slow diffusion during the long postdischarge period. Preliminary time-resolved measurements[19] have confirmed that high energy ions are observed exclusively when the pulse is on whereas the low energy group is observed mainly in the post discharge. Figure 5(b) shows IEDF of Ti^{2+} ions. The distribution can be approximated with a single Maxwellian with an effective temperature of 0.2 eV. The observed fraction of Ti^{2+} constitutes less than 1% of measured Ti^{1+} ions at this pressure.

The IEDF of Ar^{1+} [Fig. 5(c)] consists of low energy ions with energy less than 3 eV and the majority of Ar^{1+} ions have $k_BT=0.18$ eV. The effective temperatures of Ar^{1+} and low energy Maxwellian for Ti^{1+} are quite similar, indicating an equilibrium is established between gas and metal ions in the postdischarge plasma. Finally, as shown in Fig. 5(d), only a trace of low energy ($k_BT=0.2$ eV) Ar^{2+} ions is present in the discharge.

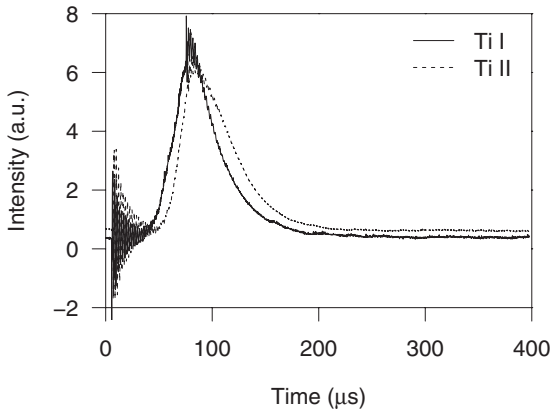

FIG. 6. Temporal evolution of optical emission observed for neutral (Ti I at 363.55 nm) and ion (Ti II at 338.38 nm) lines.

C. Temporal evolution of metal ion-to-metal neutral ratio

So far, the results obtained with Langmuir probe and mass spectroscopy measurements provided information concerning charged particles in plasma. To obtain data regarding neutral species in the discharge, time-resolved OES and AAS experiments were carried out. Figure 6 shows the temporal evolution of optical plasma emission at $I_d=20$ A. Both Ti ion (Ti II) and neutral (Ti I) intensities are very similar. Assuming both species are produced in the same way by direct electron collision from the titanium neutral ground state, this means that titanium neutral and ion ground state densities are equal and that the ion-to-neutral ratio is close to unity.

Figure 7 shows the experimentally determined absorption coefficient for neutral (Ti I) and ionized (Ti II) titanium as a function of time at $I_d=200$ A. In the first 100 μs, the absorption coefficient for Ti neutral $A_k(Ti^0)$ is close to zero indicating that the metal plasma is still mainly located at the target. As the plasma diffuses into the observation volume, $A_k(Ti^0)$ starts to increase and at 200 μs approaches a stable value. It was not possible to obtain reliable data for $A_k(Ti^{1+})$ for the first 100 μs since the plasma emission intensity was much higher than the lamp intensity. However, in the postdischarge, a stable value was observed. It should be noted that the time scale of the plasma arrival to the substrate is in a good agreement with Langmuir probe measurements taken at the same distance from the target.

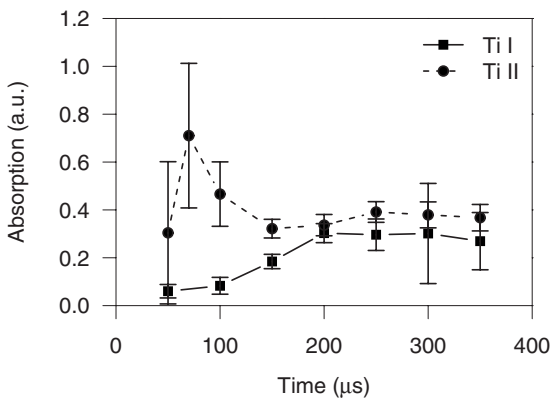

FIG. 7. Absorption coefficient of titanium neutrals (Ti I at 363.55 nm) and ions (Ti II at 338.38 nm) as a function of time.

TABLE I. Density of ions and neutrals calculated from AAS measurements.

Species	Temperature (K)	Density (10^{16} m^{-3})
Ti	300	1.4
Ti^{1+}	1000	1.5
Ti^{1+}	300	1.4

At $t=300$ μs, the absorption coefficient was estimated to be $A_k(Ti^{1+}) \sim 0.37$ for titanium ions and $A_k(Ti^0) \sim 0.30$ for titanium atoms. From these values, absolute densities of Ti^0 and Ti^{1+} were calculated in postdischarge. Subsequently it was then possible to estimate the metal ion-to-neutral ratio, which is a key parameter for thin film growth. The results of the calculations are presented in Table I.

It should be noted that the density of titanium ions was estimated assuming that they are diffusing at room temperature ($T=300$ K) to evaluate the effect of temperature on the density calculation. However, this modification did not affect significantly the resulting density value. Thus, it can be seen that the ion-to-neutral ratio is close to unity in the afterglow plasma near the substrate.

In this study, the presence of titanium metastable atoms, which could modify the ion-to-neutral ratio, was neglected. However, De Poucques *et al.*[4] reported that Ti (metastable) are ~20% of the Ti neutral density. Furthermore, metastables were only detected during the pulse and their density dropped quickly in the postdischarge due to collisions with the gas.[4] Nevertheless, it is assumed that the ion-to-neutral ratios could be overestimated by 20%; however, the dependence of ion-to-neutral ratio on discharge current is not affected.

D. Influence of discharge current on plasma composition

It is important to understand how changes in the discharge current influence the properties of plasma. The peak value I_d of the pulse current was used as representative. This was proportional to the average current in the pulse and the average current in the discharge because the current shapes were similar. As discussed earlier, the plasma arrives at the measurement plane with some delay with respect to the application of the pulse at the target.

Figure 8 is a log-log plot of I_d versus peak value n_e of the plasma density in the pulse. n_e can be considered as proportional to the total ion dose generated within the pulse assuming that main metal-containing plasma is fully formed at the end of the pulse and neglecting nonlinear plasma losses on the way to the probe. As shown in Fig. 8, n_e increases linearly (slope=1) with I_d. This may be explained by describing the ion current to the target using the Bohm presheath relation as[20]

$$I_d = 0.61 n_e e S \sqrt{\frac{kT_e}{M}}, \tag{8}$$

where n_e is plasma density, e is electron charge, S is target area, T_e is electron temperature, and M is ion mass. Assuming that the electron temperature does not vary significantly

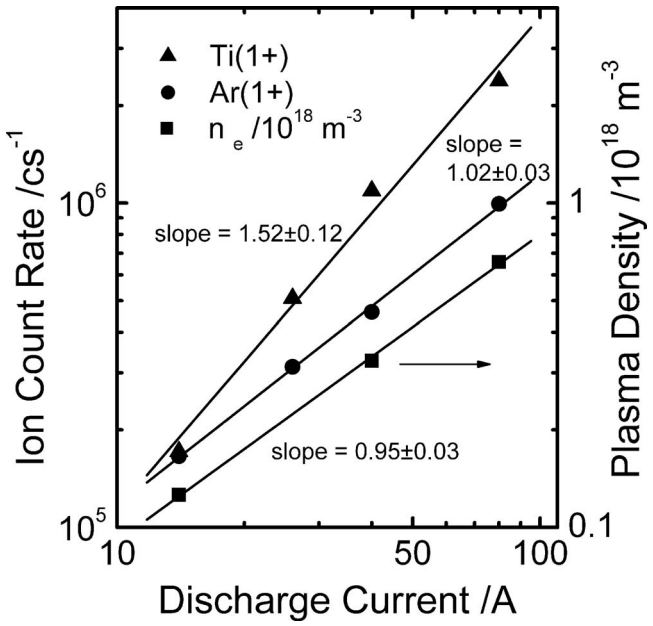

FIG. 8. Flux of Ar^{1+} and Ti^{1+} and total plasma density n_e as a function of peak discharge current

at peak I_d, the total plasma density is then directly proportional to the discharge current.

The plasma in these conditions comprises mainly singly charged Ti^{1+} and Ar^{1+} ions. Higher charge states of Ti^{2+} and Ar^{2+} were found at levels below 10%. The composition of the plasma can be estimated from the time averaged IEDFs after integration with respect to energy. Figure 8 displays the integrated count rates for Ti^{1+} and Ar^{1+} as a function of I_d. The respective rates of increase can be described quite well by the following relations:

$$n(Ti^{1+}) = CI_d^{1.5}, \tag{9}$$

$$n(Ar^{1+}) = CI_d^{1.0}, \tag{10}$$

where the C is a constant and the exponents correspond to the slopes in the log-log representation in Fig. 8.

Ti^{1+} ions may be produced in several ways. The amount of Ti^{1+} generated from the recombination of Ti^{2+} via three-body collisions or charge transfer with Ar may be neglected because only small amount (~10%) of Ti^{2+} is created at the target. Charge transfer between metastable Ar^* and Ti^0 leading to creation of Ti^{1+} is probable; however, de Poucques *et al.*[4] measured that the lifetime of Ar^* in HIPIMS postdischarges at 2.66 Pa is less than 100 μs and is thus significantly shorter than the pulse duration of the ion flux of >500 μs. Thus, most of metal ions in the discharge are created via direct electron impact ionization during the pulse. The Ti^{1+} spatial density is proportional to the electron density in the plasma and at the end of the pulse is given by[21]

$$n(Ti^{1+}) = n(Ti^0) n_e \int \sigma(\varepsilon)\rho_e(\varepsilon) v d\varepsilon = n(Ti^0) n_e g(T_e, \sigma), \tag{11}$$

where $n(Ti^0)$ is the neutral Ti density, n_e is the electron density, $\sigma(\varepsilon)$ is the energy-dependent ionization cross-section,

$\rho_e(\varepsilon)$ is the electron energy distribution, and v is the electron velocity. Combining Eqs. (11) and (8) the metal ion-to-neutral ratio $n(\mathrm{Ti}^{1+}):n(\mathrm{Ti}^0)$ can be seen to increase linearly with discharge current and plasma density.

The number of sputtered atoms is determined by the sputtering by gas ions and self-sputtering. However, the sputtering yield and self-sputtering yield are similar for metals that have similar mass to the sputtering gas. Therefore, the number of sputtered Ti metal atoms may be given as[21]

$$n(\mathrm{Ti}^0) = bYI_d = 0.61bYn_eS\sqrt{\frac{kT_e}{M}}, \tag{12}$$

where b is geometrical constant, Y is sputtering yield, S is the area of the target, M is the atomic mass of Ti, and k is Boltzmann's constant. For materials significantly heavier than Ar, the estimation would need to account for the higher self-sputter yield as well as the higher metal ion-to-gas ion ratio, which would lead to a net increase in neutral density. At the same time, however, the increased density of metal vapor would increase the density of plasma and may not necessarily result in a reduction of the ionization degree. For the particular case of Ti and other similar mass metals, Eq. (10) can be rearranged as

$$n(\mathrm{Ti}^{1+}) = bY\frac{1}{0.61S}\sqrt{\frac{M}{kT_e}}g(T_e,\sigma)I_d^2 = \mathrm{CI}_d^2. \tag{13}$$

Equation (13) shows that the density of Ti^{1+} therefore depends not only on the discharge current but also on T_e. The influence of discharge current on electron temperature was already discussed in relation to Fig. 4. It is interesting to note that T_e decreases with discharge current. For the purpose of this paper, we will neglect changes in T_e and consider $T_e^{-0.5}g(T_e,\sigma)$ a constant incorporated within C in Eq. (13).

Although the calculations predict a square law dependence, the experimental data fits well with an exponent of 1.52 [Eq. (9)]. Similar discrepancy was found in the cases of Cr, Nb, and V. Rossnagel and Saenger[21] reported a reduction of the slope at high discharge currents in conventional dc magnetron sputtering, which they suggest is attributed to gas and metal rarefaction due to heating. Furthermore, Rossnagel and Saenger[21] suggest that an increased electron temperature may be responsible; however, this is contrary to the findings for HIPIMS where T_e is decreased. Therefore, careful analysis is required to establish the roots of the discrepancy; however, this is beyond the scope of the current paper.

Figure 9 presents the influence of I_d on plasma composition as derived from mass spectroscopy and AAS. The titanium ion-to-neutral ratio monotonically increases with the discharge current.

Then, neglecting the amount of higher charged ion states such as Ar^{2+} and Ti^{2+} in plasma, the density of Ar^{1+} ions may be expressed as

$$n(\mathrm{Ar}^{1+}) = n_e - n(\mathrm{Ti}^{1+}) \sim I_d - \mathrm{CI}_d^{1.5}. \tag{14}$$

Thus, combining with Eq. (9), the metal ion-to-gas ion ratio is given by

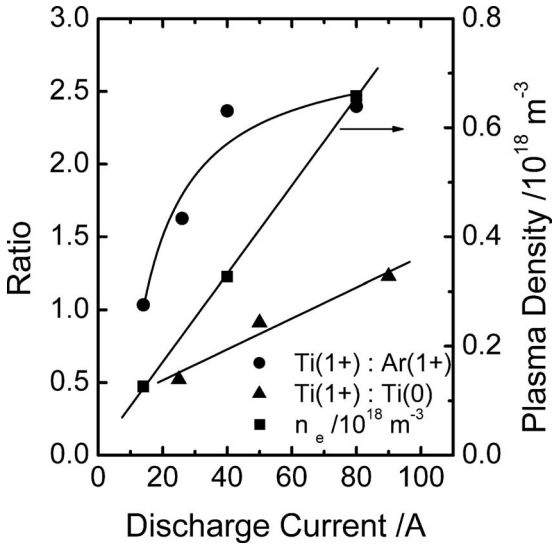

FIG. 9. Influence of I_d on plasma composition and density of HIPIMS of Ti discharges as derived from mass spectroscopy, AAS and Langmuir probe measurements.

$$\frac{n(\mathrm{Ti}^{1+})}{n(\mathrm{Ar}^{1+})} = \frac{\mathrm{CI}_d^{0.5}}{1-\mathrm{CI}_d^{0.5}} + D, \tag{15}$$

where D is a constant. This function increases quickly at low I_d and finally saturates to a steady state. By fitting the constants C and D, one can obtain a reasonable approximation to the measured data, as shown in Fig. 8.

IV. CONCLUSIONS

Plasma density and composition of HIPIMS of Ti discharge at the position of the substrate were determined successfully by Langmuir probe measurements, energy-resolved mass spectroscopy, and AAS. It was shown that the discharge current increases the overall plasma density, the metal ion-to-gas ion ratio, and the metal ion-to-neutral ratio. At a discharge current density of 1 A cm^{-2}, the ratio of $\mathrm{Ar}^{1+}:\mathrm{Ti}^{1+}:\mathrm{Ti}^0$ was approximately 2:1:1 at a plasma density of 4×10^{17} m^{-3}. It was found that the plasma density and metal ionization degree ($\mathrm{Ti}^{1+}:\mathrm{Ti}^0$ ratio) were directly proportional to the target current, whereas the gas ion-to-metal ion ratio $\mathrm{Ti}^{1+}:\mathrm{Ar}^{1+}$ reached a saturation point at high currents. This was shown to be consistent with electron impact ionization as the main mechanism.

ACKNOWLEDGMENTS

The authors would like to acknowledge the financial support of EPSRC Grant No. EP/D049202/1 and EU project INNOVATIAL.

[1] A. P. Ehiasarian, W.-D. Munz, L. Hultman, U. Helmersson, and I. Petrov, Surf. Coat. Technol. **163–164**, 267 (2003).
[2] P. Eh. Hovsepian, C. Reinhard, and A. P. Ehiasarian, Surf. Coat. Technol. **201**, 4105 (2006).
[3] Y. P. Purandare, A. P. Ehiasarian, and P. Eh. Hovsepian, J. Vac. Sci. Technol. A **26**, 288 (2008).
[4] L. de Poucques, J. C. Imbert, C. Boisse-Laporte, J. Bretagne, M. Ganciu, L. Teule-Gay, and M. Touzeau, Plasma Sources Sci. Technol. **15**, 661 (2006).
[5] S. Konstantinidis, J. P. Dauchot, M. Ganciu, A. Ricard, and M. Hecq, J.

Appl. Phys. **99**, 013307 (2006).
[6]J. T. Gudmundsson, J. Alami, and U. Helmersson, Surf. Coat. Technol. **161**, 249 (2002).
[7]A. P. Ehiasarian, R. New, W.-D. Münz, L. Hultman, U. Helmersson, and V. Kouznetsov, Vacuum **65**, 147 (2002).
[8]J. Bohlmark, M. Lattemann, J. T. Gudmundsson, A. P. Ehiasarian, Y. Aranda-Gonzalvo, N. Brenning, and U. Helmersson, Thin Solid Films **515**, 1522 (2006).
[9]A. P. Ehiasarian, Y. Aranda Gonzalvo, and T. D. Whitmore, Plasma Processes Polym. **4**, S309 (2007).
[10]J. Vlcek, A. D. Pajdarova, and J. Musil, Contrib. Plasma Phys. **44**, 426 (2004).
[11]J. Böhlmark, J. Alami, C. Christou, A. P. Ehiasarian, and U. Helmersson, J. Vac. Sci. Technol. A **23**, 18 (2005).
[12]M. J. Druyvesteyn, Z. Phys. **64**, 781 (1930).
[13]V. A. Godyak, R. B. Piejak, and B. M. Alexandrovich, J. Appl. Phys. **73**, 3657 (1993).
[14]S. Konstantinidis, A. Ricard, M. Ganciu, J. P. Dauchot, C. Ranea, and M. Hecq, J. Appl. Phys. **95**, 2900 (2004).
[15]K. Macak, V. Kouznetsov, J. Schneider, U. Helmersson, and I. Petrov, J. Vac. Sci. Technol. A **18**, 1533 (2000).
[16]S. Konstantinidis, J. P. Dauchot, M. Ganciu, and M. Hecq, Appl. Phys. Lett. **88**, 021501 (2006).
[17]A. Vetushka and A. P. Ehiasarian, J. Phys. D **41**, 015204 (2008).
[18]A. Anders, IEEE Trans. Plasma Sci. **29**, 393 (2001).
[19]A. Hecimovic, K. Burcalova, and A. P. Ehiasarian, J. Phys. D **41**, 095203 (2008).
[20]B. Chapman, *Glow Discharge Processes* (Wiley, New York, 1980).
[21]S. M. Rossnagel and K. L. Saenger, J. Vac. Sci. Technol. A **7**, 968 (1989).